Layer-exchange crystallization for low-temperature (~450° C) formation of n-type tensile-strained Ge on insulator

Gao, Hongmiao
Department of Electronics, Kyushu University

Sadoh, Taizoh
Department of Electronics, Kyushu University

出版情報：Applied Physics Letters. 117 (17), pp.172102-, 2020-10-26. AIP Publishing
バージョン：

Applied Physics Letters ARTICLE scitation.org/journal/apl

Layer-exchange crystallization for low-temperature (∼450 °C) formation of n-type tensile-strained Ge on insulator

Cite as: Appl. Phys. Lett. **117**, 172102 (2020); doi: 10.1063/5.0020489
Submitted: 1 July 2020 · Accepted: 12 October 2020 ·
Published Online: 26 October 2020

Hongmiao Gao and Taizoh Sadoh[a)]

AFFILIATIONS

Department of Electronics, Kyushu University, 744 Motooka, Fukuoka 819-0395, Japan

[a)]Author to whom correspondence should be addressed: sadoh@ed.kyushu-u.ac.jp

ABSTRACT

Layer-exchange crystallization of Ge using a group-V element has been investigated to develop a low-temperature (<500 °C) formation technique of n-type tensile-strained crystalline Ge on insulator. Here, the Sb of a group-V element is employed as a catalyst. Annealing (450 °C) of a-Ge (100 nm)/Sb (100 nm) bi-layer stacked structures generates layer-exchange crystallization. Namely, Ge and Sb layers exchange their positions, and Ge layers are crystallized on insulator substrates. However, Ge evaporation occurs during annealing, and a high concentration of Sb (∼20%) remains at the Ge/insulator interface. To solve these problems, the thickness reduction of Sb films and introduction of a-Ge thin under-layers are examined. By annealing (450 °C) a-Ge (100 nm)/Sb (50 nm)/a-Ge (5 nm) tri-layer structures, layer-exchange crystallization of Ge layers on insulator without Ge evaporation or Sb residue has been achieved. This enables formation of n-type tensile-strained (∼0.3%) Ge layers (free electron concentration: $\sim 5 \times 10^{17}$ cm^{-3}). Moreover, crystal orientation control of grown Ge films through the introduction of the diffusion barrier is examined. These results demonstrate the possibility of layer-exchange crystallization induced by a group-V element to realize functional thin-film devices for advanced electronics and photonics.

Germanium (Ge) is a promising material for the realization of next-generation large-scale integrated circuits (LSIs) because Ge has high carrier mobility[1–4] and superior optical properties[5–8] compared to Si. To merge Ge-based high-speed transistors and high-efficiency optical devices onto LSIs, the development of formation techniques of Ge on insulator with a low-thermal budget (<500 °C) is essential. Thus, low-temperature growth of Ge-on-insulator (GOI) has been intensively investigated.[9] In line with this, various techniques such as solid-phase crystallization (SPC),[10–13] metal-induced lateral crystallization,[14,15] metal-induced layer-exchange crystallization,[16–20] and laser annealing[21,22] have been developed.

Among them, metal-induced layer-exchange crystallization using stacked structures of amorphous semiconductors and catalytic metals is attracting much attention.[16–20,24,25] Previously, we investigated layer-exchange crystallization of Si, Ge, and SiGe using various metals such as Al[17,23] and Au[19,20,24] and achieved (111)- or (100)-oriented large-grain (≥50 μm) crystals on insulator at low temperatures (e.g., ≤500 °C for Al and ∼250 °C for Au) by combining inter-diffusion control between the semiconductor and metal layers. Such large-grain growth with controlled crystal orientation is a big advantage of the layer-exchange technique. In addition, based on these previous results, we clearly showed that layer-exchange crystallization proceeds only for stacked structures of amorphous semiconductors and the metals, which form eutectics with the semiconductors, at a temperature below eutectic points of semiconductor-metal systems.[24]

However, all Ge films obtained in the previous works of Al- and Au-induced layer exchange processes showed p-type conduction. In semiconductor films obtained by layer-exchange crystallization, catalyst atoms with thermal equilibrium solid solubility at growth temperatures are incorporated in grown layers.[20] For example, in the case of Al-induced crystallization, holes are generated from the shallow-acceptor level of high-concentration Al atoms with thermal equilibrium solid solubility (e.g., $\sim 4 \times 10^{20}$ cm^{-3} at 400 °C) in Ge. On the other hand, in the case of Au-induced crystallization, although thermal equilibrium solid solubility of Au is low (e.g., $\sim 4 \times 10^{9}$ cm^{-3} at 250 °C), holes ($\sim 2 \times 10^{17}$ cm^{-3}) are generated from the shallow-acceptor level of vacancy-related defects in Ge.[20]

For device application, n-type Ge is also necessary. One of the attractive points of n-type Ge is high-efficiency optical properties owing to the high electron population in the Γ band.[5,7] Sun *et al.*

reported that n-type doping above $\sim 5 \times 10^{17}\,cm^{-3}$ enhanced photoluminescence of tensile-strained (~0.2%) Ge.[5] Thus, the development of formation techniques of n-type Ge by layer-exchange crystallization is desired. For this purpose, we propose an Sb of a group V element as the catalyst for layer-exchange crystallization of Ge because Sb forms eutectic with Ge at 592 °C.[26] Recently, SPC[27] and laser annealing[28] of Sb-doped Ge were investigated, and very promising results were reported. However, the possibility of layer-exchange crystallization using a group V element has not been clarified yet.[25] In the present study, we examine Sb-induced layer-exchange crystallization of Ge on insulator.

Bi-layer sample structures illustrated in Fig. 1(a) are examined for the initial trial. Stacked structures of a-Ge (thickness: 100 nm)/Sb (thickness: 100 nm) were formed on fused-quartz (SiO_2) substrates at room temperature, where Sb and Ge were deposited by thermal evaporation (base pressure: $\sim 1 \times 10^{-6}$ Torr) and molecular-beam techniques (base pressure: $\sim 5 \times 10^{-10}$ Torr), respectively. Samples were annealed in N_2. The grown layers were analyzed by micro-probe Raman spectroscopy (laser spot diameter: ~1 μm, wavelength: 532 nm, and laser power: 200 mW) and Auger electron spectroscopy (AES).

Raman spectra of samples before and after annealing at 300 °C (100 h), 400 °C (20 h), and 450 °C (20 h) are shown in Fig. 1, where measurements were performed from the backside of samples through

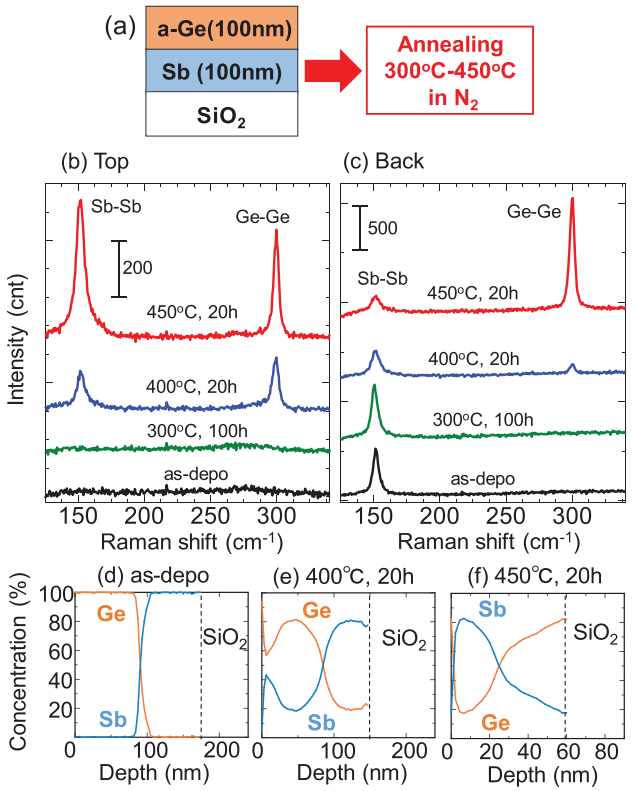

FIG. 1. Schematics of the bi-layer sample structure for the initial trial (a), Raman spectra obtained from top side (b) and backside (c) of samples before and after annealing at 300 °C (100 h), 400 °C (20 h), and 450 °C (20 h), and in-depth profiles of Ge and Sb concentrations in samples before (d) and after annealing at 400 °C (20 h) (e) and 450 °C (20 h) (f). The thicknesses of the a-Ge and Sb films are 100 and 100 nm, respectively.

transparent substrates [Fig. 1(c)] as well as from the top side [Fig. 1(b)]. Before annealing, no Raman peak is observed from the top side as shown in Fig. 1(b), indicating that the top Ge layer is amorphous. On the other hand, a peak due to Sb–Sb bonding in crystalline Sb is observed at $\sim 150\,cm^{-1}$ from the backside [Fig. 1(c)], indicating that the bottom Sb layer is the crystal. After annealing at 300 °C, no change is observed in Raman spectra. However, upon increasing annealing temperature above 400 °C, Fig. 1(c) shows that intensities of Raman peaks due to Sb–Sb bonding decrease and a large peak due to Ge–Ge bonding in crystalline Ge appears at $\sim 300\,cm^{-1}$ after annealing at 450 °C. On the other hand, in Raman spectra observed from the top side [Fig. 1(b)], a large Raman peak due to Sb–Sb bonding appears after annealing at 450 °C. These results suggest the movement of Ge and Sb atoms from the top to the bottom layers and from the bottom to the top layers, respectively, and formation of crystalline Ge films in the bottom layer at 450 °C.

In-depth concentration profiles in samples are analyzed by AES measurements. The results of the samples before and after annealing at 400 °C (20 h) and 450 °C (20 h) are shown in Figs. 1(d)–1(f), respectively. Figure 1(d) shows that a bi-layer Ge/Sb stacked structure as shown in Fig. 1(a) is formed before annealing. After annealing at 400 °C, the Ge/Sb interface becomes broad, as shown in Fig. 1(e). This indicates that inter-diffusion of Ge and Sb occurs at 400 °C. After annealing at 450 °C, Sb and Ge become dominant constituents in the top and bottom layers, respectively, as shown in Fig. 1(f), which indicates that dominant constituents in the top layer and the bottom layers have been exchanged by annealing.

These results of Raman and AES measurements clearly indicate that the layer-exchange crystallization is generated by annealing at 450 °C (20 h). However, as shown in Fig. 1(f), the total film thickness of the annealed sample (450 °C, 20 h) is decreased from ~200 nm to ~60 nm, i.e., about one third of the initial thickness, which is attributed to thermal evaporation during annealing. Moreover, Sb atoms with a high concentration (~20%) remain at the bottom-layer/substrate interface due to insufficient layer exchange.

The vapor pressure of Sb at the annealing temperature (450 °C) is as high as about 3×10^{-4} Torr.[29] On the other hand, the vapor pressure of Ge is less than 10^{-10} Torr at 450 °C.[29] In addition, evaporation of Ge was not observed in SPC of pure Ge films on insulator at a temperature of ~450 °C.[10,11] The present results suggest that evaporation of Ge is induced by high-concentration Sb. We speculate that Sb atoms are introduced into Ge layers during annealing and weaken the bonding between Ge atoms, which generates thermal evaporation of Ge together with Sb during annealing at 450 °C. Thus, the decrease in the Sb thickness is expected to be useful to suppress the Ge evaporation. On the other hand, it is reported that introduction of a thin Ge underlayer into the initial catalyst/substrate interface enhances the layer-exchange crystallization in Al-induced crystallization.[18] The introduction of a thin a-Ge underlayer will also be useful to enhance the layer exchange in Sb-induced crystallization, which will result in the decrease in the residual Sb atoms at the bottom layer/substrate interface.

Therefore, we examine the modified sample structure of tri-layers, as shown in Fig. 2(a). The thickness of the Sb film is decreased to 50 nm, and a thin a-Ge underlayer (0 – 5 nm) is inserted between the Sb layer and the substrate. The Ge underlayers were formed using the thermal evaporation system, and deposition of the Sb films was

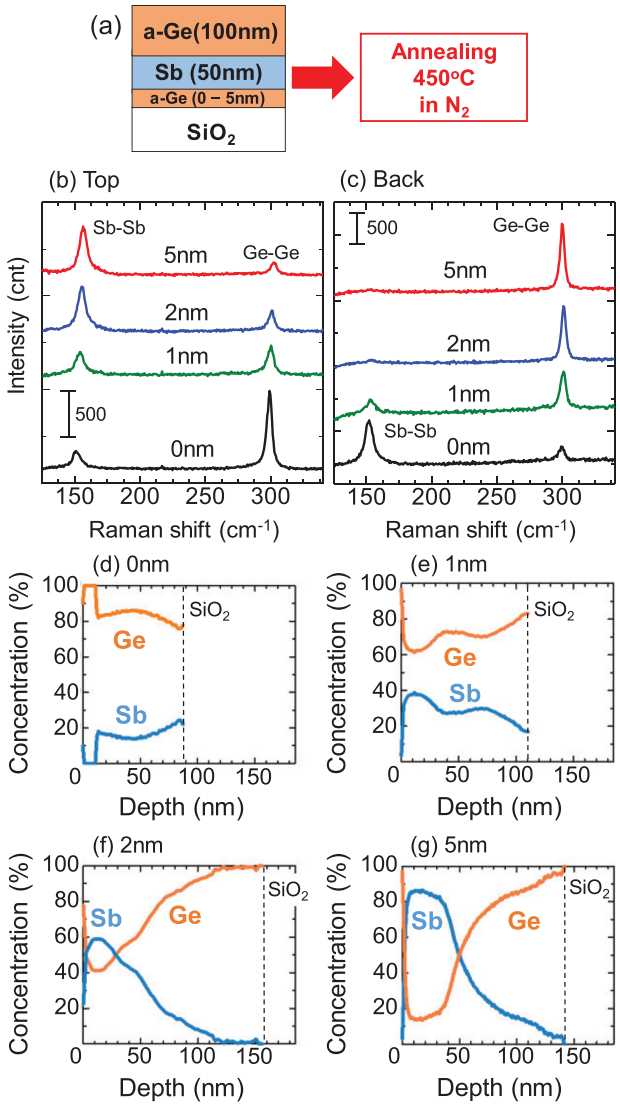

FIG. 2. Schematics of the tri-layer sample structure (a), Raman spectra obtained from top side (b) and backside (c) of samples after annealing (450 °C, 20 h), where the film thicknesses of the top a-Ge, Sb, and underlayer a-Ge are 100, 50, and 0 – 5 nm, respectively, and composition profiles of samples with Ge underlayer thicknesses of 0 (d), 1 (e), 2 (f), and 5 nm (g) after annealing (450 °C, 20 h).

performed in the same chamber without breaking vacuum. The deposition of the top Ge films was performed in the molecular-beam deposition system, where the samples were exposed to air for several minutes before loading into the molecular-beam deposition chamber.

Raman spectra of the samples (underlayer thickness: 0, 1, 2, and 5 nm) after annealing (450 °C, 20 h) are shown in Figs. 2(b) and 2(c), which were obtained from the top side and backside, respectively. For samples with underlayer thicknesses of 0 and 1 nm, peaks due to Sb–Sb bonding are observed from the top side, as shown in Fig. 2(b). However, they are weak, and strong peaks due to Ge–Ge bonding are dominant, which suggests that the top Ge layers are crystallized without layer exchange. On the other hand, for underlayer thicknesses of 2 and 5 nm, strong peaks due to Sb–Sb bonding are observed from the top side, while strong peaks due to Ge–Ge bonding are observed from the backside. This suggests enhanced layer exchange for these samples (underlayer thickness: 2 and 5 nm). It is noted that the intensity of the Raman peak due to Ge–Ge bonding detected from the backside is the highest for the sample with the underlayer thickness of 5 nm.

The composition profiles of the samples (underlayer thickness: 0, 1, 2, and 5 nm) after annealing (450 °C, 20 h) are shown in Figs. 2(d)–2(g), respectively. Here, the total thicknesses (∼150 nm) of the samples (underlayer thickness: 2 and 5 nm) are almost the same as those of the initial sample structures (152 and 155 nm) though those of the other samples (underlayer thickness: 0 and 1 nm) are significantly decreased. These results indicate that thermal evaporation of the Ge films is effectively suppressed by using the modified structures with underlayer thicknesses of 2 and 5 nm. For these samples, the Sb concentrations in the top layers become higher than those in the bottom layers. The layer-exchange crystallization using a-Ge/Sb stacked structures proceeds through the following steps: (a) supply of Ge atoms into the Sb layer, (b) nucleation and subsequent growth of Ge in the Sb layer, and (c) push up of Sb atoms into the upper layer. In the present study, by introducing the Ge underlayers with thicknesses above 2 nm, step (a) is accelerated, and thus, the layer exchange is enhanced.

However, the Sb concentration in the top layer is as low as 60% for the sample with the underlayer thickness of 2 nm, as shown in Fig. 2(f). The results shown in Figs. 2(d)–2(g) indicate that layer exchange is hardly generated or insufficient for the samples with underlayer thicknesses of 0 – 2 nm, while almost completed layer exchange is achieved for the sample with the underlayer thickness of 5 nm. Moreover, there are no residual Sb atoms at the bottom-layer/substrate interface, as shown in Fig. 2(g). These results clearly demonstrate that the modified sample structure, where the Sb film thickness is decreased to 50 nm, and thin (∼5 nm) Ge underlayer is introduced, enables complete layer-exchange crystallization upon suppressing thermal evaporation of Ge during annealing and without Sb residue near the substrates. As a result, layer exchange crystallization using a group V element, which never reported previously,[25] has been realized.

To remove Sb atoms in the top layers, selective etching of Sb was examined using a diluted *aqua regia* for the sample (a-Ge/Sb/a-Ge thickness: 100/50/5 nm) after annealing (450 °C, 20 h). To monitor the Sb residue in the top layers, Raman measurements were performed from the top side of the samples. Raman spectra obtained before and after etching for 60, 120, and 180 s are shown in Fig. 3(a). This figure shows that the intensities of the Raman peaks due to Sb–Sb bonding decrease with the increasing etching time, and the Sb–Sb peak becomes very small after etching for 180 s. The Ge and Sb concentration profiles obtained by AES analysis for the sample after etching of Sb (etching time: 180 s) are shown in Fig. 3(b), which reveals that the concentration of residual Sb in a wide region of the Ge layer (depth: 20 – 50 nm) is under the detection limit (∼1%) though a small amount of Sb atoms (<20%) remain in the surface region (depth: 0 – 20 nm) due to insufficient etching. This result indicates that almost all the Sb atoms existing in the bottom layer before etching were removed by etching by preserving the Ge region. This phenomenon is

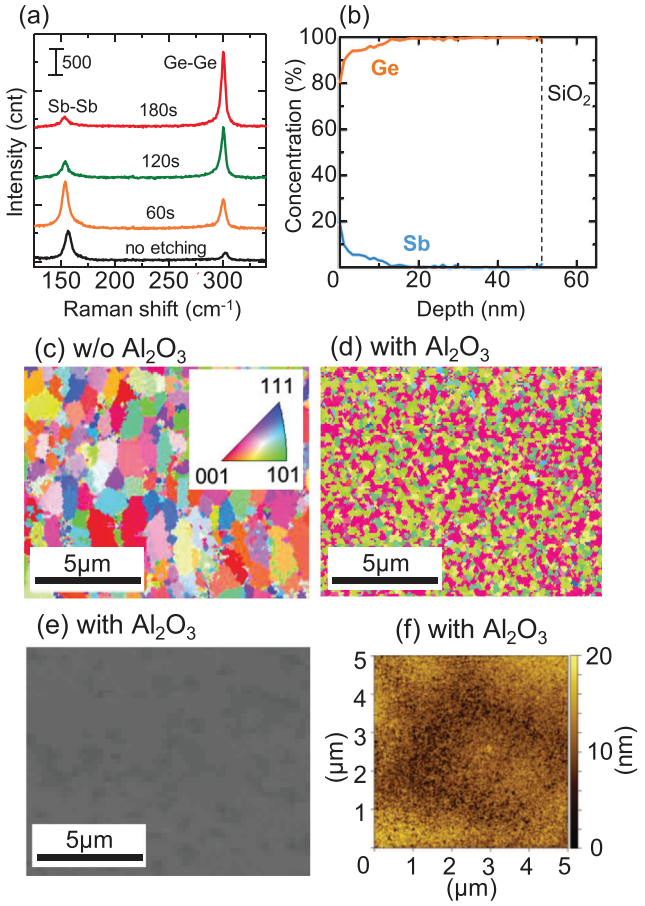

FIG. 3. Raman spectra (a), composition profiles (b), and EBSD image (c) of the tri-layer sample (a-Ge/Sb/a-Ge = 100/50/5 nm, annealing: 450 °C, 20 h); EBSD (d), SEM (e), and AFM images (f) of the tri-layer sample introduced with the diffusion barrier (a-Ge/Al_2O_3/Sb/a-Ge = 100/0.5/50/5 nm, annealing: 450 °C, 100 h) after etching. The etching times (0 – 180 s) for (a) are indicated in the figure, and those for (b)–(f) are 180 s.

attributed to the fact that the Sb atoms in the bottom layer existed at grain boundaries of Ge before etching and were removed by etching. Analysis of the position of the Raman peak due to Ge–Ge bonding showed a tensile strain (~0.3%) for the sample (etching time: 180 s). The introduction of the tensile strain is attributed to the difference in the thermal expansion between the Ge layer and the substrate (SiO_2) by cooling from 450 °C to room temperature.

It is noted that the total thickness of the Ge films is decreased to ~50 nm after etching, as shown in Fig. 3(b). To obtain thicker Ge films, it is useful to increase the thickness of the starting a-Ge films. For Al-induced layer-exchange crystallization, growth employing thicker a-$Si_{1-x}Ge_x$ films (~500 nm) is demonstrated,[30,31] as well as thin films (~50 nm).[17,18] This indicates that the thicknesses of semiconductor films employed in layer exchange processes can be scaled up. We expect that thicknesses of Ge films obtained by Sb-induced crystallization and subsequent etching can also be increased by thickening the starting a-Ge films.

Crystal structures of the grown Ge films were analyzed using electron backscattering diffraction (EBSD) measurements, where Sb layers were removed by etching before the EBSD measurements. The EBSD image indicating crystal orientations normal to the surface of the sample (a-Ge/Sb/a-Ge thickness: 100/50/5 nm) after annealing (450 °C, 20 h) is shown in Fig. 3(c). This image shows that the grown Ge film consists of randomly oriented crystal grains with diameters of ~2 μm. This result agrees with reports of Al-induced crystallization and Au-induced crystallization without the diffusion barrier between catalytic metal layers and semiconductor layers, where randomly oriented bulk nucleation in metal layers is dominant.[17–19,23]

For crystal-orientation control of Ge films, introduction of a diffusion barrier into the interface between the top a-Ge and Sb layers is investigated. By introduction of the diffusion barrier, supply of Ge atoms into Sb layers becomes moderately slow, which will result in suppression of randomly oriented bulk nucleation and domination of preferentially oriented interface nucleation.[17–19,23] To examine this, the diffusion barrier of thin amorphous Al_2O_3 layers (thickness: 0.5 nm) was introduced into the interface between the top a-Ge (thickness: 100 nm) and Sb layers (thickness: 50 nm), where amorphous Al_2O_3 layers were deposited by sputtering.

The EBSD image indicating crystal orientations normal to the surface of the sample (a-Ge/Al_2O_3/Sb/a-Ge thickness: 100/0.5/50/5 nm) after annealing (450 °C, 100 h) is shown in Fig. 3(d). Although the image is composed of small domains (diameters: ~1 μm), the whole area is covered with only two colors, i.e., red and green, which indicate (001) and (101), respectively. From detailed analysis of the EBSD data, it was found that almost all the in-plane crystal directions of the red domains, having (001)-oriented surfaces, were aligned to one direction, and those of the green domains, having (101)-oriented surfaces, were aligned to another direction.

Interestingly, the whole area shown in Fig. 3(d) consists of (001) and (101)-oriented domains, where the in-plane crystal directions are regularly aligned to each other with a constant angle. We discuss these crystal orientations on the basis of the preferentially oriented interface nucleation of Ge at Al_2O_3/Sb interfaces. It is reported that amorphous Al_2O_3 layers are partially crystallized into the γ-phase at 450 °C.[32] Namely, the Al_2O_3 diffusion barriers employed in the present study heterogeneously consist of an amorphous phase and a crystal γ-phase formed during annealing (450 °C, 100 h). Preferentially, (001)-oriented nucleation of Ge is dominant on amorphous Al_2O_3, due to minimization of interface energy.[19,33] This should result in generation of a (001)-oriented Ge nucleus in the initial stage of the annealing and subsequent growth of a (001)-oriented domain. On the other hand, the origin of the (101)-oriented domain can be attributed to twin formation on γ-phase Al_2O_3 during the lateral growth from the (001)-oriented domain. With the increasing annealing time, twin formation of (001)-oriented domains on amorphous Al_2O_3 and (101)-oriented domains on γ-phase Al_2O_3 proceeds repeatedly, and the whole area is covered with (001) and (101)-oriented domains, as shown in Fig. 3(d). It is reported that carrier scattering at twin boundaries is much smaller compared to randomly oriented grain boundaries.[34]

These results suggest possibility of orientation control of grown Ge films by employing preferentially oriented interface nucleation. To achieve complete control of crystal orientations and remove twin boundaries, the growth temperature should be decreased below 300 °C to suppress formation of the crystal γ-phase.[32] Recently, we

investigated Al-induced crystallization of Sn-doped Ge and found that the growth temperature of Al-induced crystallization decreased from 400 °C to 250 °C by doping with a small amount of Sn (2%) into a-Ge.[35] To decrease the growth temperature in Sb-induced crystallization, Sn doping into the top a-Ge layers will be useful.

Surface morphologies of the grown layers are analyzed using scanning electron microscopy (SEM) and atomic force microscopy (AFM). Figures 3(e) and 3(f) show the SEM and AFM images of the sample after Sb etching (etching time: 180 s), respectively. The arithmetic average value of roughness (Ra) obtained from the AFM measurement is as small as 1.9 nm. These results indicate that the surfaces of the grown layers are flat.

Hall effect measurements were performed for the grown samples after Sb etching (etching time: 180 s) using the van der Pauw method. The results for the sample (a-Ge/Sb/a-Ge thickness: 100/50/5 nm) after annealing (450 °C, 20 h) showed that the grown Ge films were n-type conduction with a free electron concentration of $\sim 5 \times 10^{17}\,\mathrm{cm}^{-3}$ and a mobility of $\sim 70\,\mathrm{cm}^2\,\mathrm{V}^{-1}\,\mathrm{s}^{-1}$. The value of the free electron concentration is smaller than the thermal equilibrium solid solubility ($\sim 3 \times 10^{18}\,\mathrm{cm}^{-3}$) of Sb in Ge at 450 °C, which was obtained by extrapolation of the reported data at temperatures above 600 °C.[36] We speculate that the low concentration of free electrons in the grown Ge films is mainly caused by compensation by high concentration acceptors originated from vacancy-related defects and grain boundaries in Ge.[10,37,38] It is reported that these defects in poly-Ge films are reduced by post-annealing.[10,39] Thus, the free electron concentration will be increased through defect reduction by post-annealing. On the other hand, the sample (a-Ge/Al_2O_3/Sb/a-Ge thickness: 100/0.5/50/5 nm) after annealing (450 °C, 100 h) showed n-type conduction by the thermoelectric probe method. However, it was difficult to evaluate the free electron concentration and mobility by the Hall effect measurements, probably due to insufficient Ohmic contacts. Detailed characterization of the grown Ge layers is now under way.

In summary, we have investigated layer-exchange crystallization using a group-V element. Annealing (450 °C, 20 h) of a-Ge (100 nm)/Sb (100 nm) bi-layer stacked structures generated layer-exchange crystallization though Ge evaporation and Sb residue at the bottom-layer/substrate interfaces were observed. To solve these problems, we have modified the sample structures, i.e., a decrease in the Sb film thickness to 50 nm and introduction of thin a-Ge underlayers. Employment of the tri-layer stacked structures [a-Ge (100 nm)/Sb (50 nm)/a-Ge (5 nm)] enables complete layer-exchange growth without Ge evaporation or Sb remaining at the bottom-layer/substrate interfaces. As a result, n-type tensile-strained (~0.3%) Ge films (free electron concentration: $\sim 5 \times 10^{17}\,\mathrm{cm}^{-3}$) on insulator have been obtained at a low temperature (~450 °C). Moreover, the possibility of crystal orientation control of grown Ge films by introduction of the diffusion barrier (thin Al_2O_3 layers) is obtained. This technique will facilitate realization of advanced LSIs merged with functional thin-film devices.

The authors wish to thank Professor T. Asano and Mr. T. Kajiwara of Kyushu University for providing the opportunity to use the EBSD analysis system and for performing the AFM measurements, respectively. Part of this work was supported by a Grant-in-Aid (Nos. JP15H03976, JP16K14234, and JP19K21976) for Scientific Research from the Ministry of Education, Culture, Sports, Science, and Technology in Japan.

DATA AVAILABILITY

The data that support the findings of this study are available from the corresponding author upon reasonable request.

REFERENCES

[1]M. Miyao, E. Murakami, H. Etoh, K. Nakagawa, and A. Nishida, J. Cryst. Growth **111**, 912 (1991).
[2]K. C. Saraswat, C. Chui, T. Krishnamohan, A. Nayfeh, and P. McIntyre, Microelectron. Eng. **80**, 15 (2005).
[3]R. Zhang, P.-C. Huang, J.-C. Lin, N. Taoka, M. Takenaka, and S. Takagi, IEEE Trans. Electron Devices **60**, 927 (2013).
[4]A. Toriumi and T. Nishimura, Jpn. J. Appl. Phys., Part 1 **57**, 010101 (2018).
[5]X. Sun, J. Liu, L. C. Kimerling, and J. Michel, Appl. Phys. Lett. **95**, 011911 (2009).
[6]D. Nam, D. Sukhdeo, S.-L. Cheng, A. Roy, K. C.-Y. Huang, M. Brongersma, Y. Nishi, and K. Saraswat, Appl. Phys. Lett. **100**, 131112 (2012).
[7]K. Takinai and K. Wada, J. Appl. Phys. **119**, 181504 (2016).
[8]S. A. Srinivasan, C. Porret, M. Pantouvaki, Y. Shimura, P. Geiregat, R. Loo, J. Van Campenhout, and D. Van Thourhout, Appl. Phys. Lett. **113**, 161101 (2018).
[9]M. Miyao and T. Sadoh, Jpn. J. Appl. Phys., Part 1 **56**, 05DA06 (2017).
[10]K. Toko, I. Nakao, T. Sadoh, T. Noguchi, and M. Miyao, Solid-State Electron. **53**, 1159 (2009).
[11]T. Sadoh, Y. Kai, R. Matsumura, K. Moto, and M. Miyao, Appl. Phys. Lett. **109**, 232106 (2016).
[12]K. Moto, R. Yoshimine, T. Suemasu, and K. Toko, Sci. Rep. **8**, 14832 (2018).
[13]C. Xu, X. Gong, M. Miyao, and T. Sadoh, Appl. Phys. Lett. **115**, 042101 (2019).
[14]H. Kanno, K. Toko, T. Sadoh, and M. Miyao, Appl. Phys. Lett. **89**, 182120 (2006).
[15]J.-H. Park, M. Tada, P. Kapur, H. Peng, and K. C. Saraswat, J. Appl. Phys. **104**, 064501 (2008).
[16]Z. M. Wang, J. Y. Wang, L. P. H. Jeurgens, and E. J. Mittemeijer, Phys. Rev. B **77**, 045424 (2008).
[17]M. Kurosawa, N. Kawabata, T. Sadoh, and M. Miyao, ECS J. Solid State Sci. Technol. **1**, P144 (2012).
[18]K. Toko, R. Numata, N. Oya, N. Fukata, N. Usami, and T. Suemasu, Appl. Phys. Lett. **104**, 022106 (2014).
[19]J.-H. Park, T. Suzuki, M. Kurosawa, M. Miyao, and T. Sadoh, Appl. Phys. Lett. **103**, 082102 (2013).
[20]J.-H. Park, K. Kasahara, K. Hamaya, M. Miyao, and T. Sadoh, Appl. Phys. Lett. **104**, 252110 (2014).
[21]H. Watakabe, T. Sameshima, H. Kanno, and M. Miyao, Thin Solid Films **508**, 315 (2006).
[22]W. Yeh, H. Chen, H. Huang, C. Hsiao, and J. Jeng, Appl. Phys. Lett. **93**, 094103 (2008).
[23]M. Kurosawa, T. Sadoh, and M. Miyao, J. Appl. Phys. **116**, 173510 (2014).
[24]J.-H. Park, M. Kurosawa, N. Kawabata, M. Miyao, and T. Sadoh, Electrochem. Solid-State Lett. **14**, H232 (2011).
[25]K. Toko and T. Suemasu, J. Phys. D **53**, 373002 (2020).
[26]T. B. Massalski, *Binary Alloy Phase Diagrams* (American Society for Metals, Metals Park, 1986), Vol. 2.
[27]D. Takahara, K. Moto, T. Imajo, T. Suemasu, and K. Toko, Appl. Phys. Lett. **114**, 082105 (2019).
[28]K. Takahashi, M. Kurosawa, H. Ikenoue, M. Sakashita, O. Nakatsuka, and S. Zaima, Appl. Phys. Lett. **112**, 062104 (2018).
[29]R. E. Honig, RCA Rev. **18**, 195 (1957).
[30]O. Nast, T. Puzzer, L. Koschier, A. Sproul, and S. Wenham, Appl. Phys. Lett. **73**, 3214 (1998).
[31]M. Gjukic, M. Buschbeck, R. Lechner, and M. Stutzmann, Appl. Phys. Lett. **85**, 2134 (2004).
[32]L. P. H. Jeurgens, W. G. Sloof, F. D. Tichelaar, and E. J. Mittemeijer, Thin Solid Films **418**, 89 (2002).
[33]J. Schneider, A. Sarikov, J. Klein, M. Muske, I. Sieber, T. Quinn, H. S. Reehal, S. Gall, and W. Fuhs, J. Cryst. Growth **287**, 423 (2006).

[34]N. Matsuki, R. Ishihara, A. Baiano, and K. Beenakker, Appl. Phys. Lett. **93**, 062102 (2008).
[35]M. Sasaki, M. Miyao, and T. Sadoh, in Proceedings of 23rd International Workshop on Active-Matrix Flatpanel Displays and Devices (2016), pp. 191–193.
[36]F. A. Trumbore, Bell Sys. Tech. J. **39**, 205 (1960).
[37]E. A. Fitzgerald and S. B. Samavedam, Thin Solid Films **294**, 3 (1997).
[38]H. Yang, D. Wang, and H. Nakashima, Appl. Phys. Lett. **95**, 122103 (2009).
[39]H. Kasirajan, W.-H. Huang, M.-H. Kao, H.-H. Wang, J.-M. Shieh, F.-M. Pan, and C.-H. Shen, Appl. Phys. Express **11**, 101305 (2018).